

Re(bpy)(CO)₃CN as a Probe of Conformational Flexibility in a Photochemical Ribonucleotide Reductase[†]

Steven Y. Reece,[‡] Daniel A. Lutterman,[‡] Mohammad R. Seyedsayamdost,[‡] JoAnne Stubbe,^{*,‡,§} and Daniel G. Nocera^{*,‡}

[‡]Department of Chemistry and [§]Department of Biology, Massachusetts Institute of Technology,
77 Massachusetts Avenue, Cambridge, Massachusetts 02139-4307

Received April 5, 2009; Revised Manuscript Received April 28, 2009

ABSTRACT: Photochemical ribonucleotide reductases (photoRNRs) have been developed to study the proton-coupled electron transfer (PCET) mechanism of radical transport in *Escherichia coli* class I ribonucleotide reductase (RNR). The transport of the effective radical occurs along several conserved aromatic residues across two subunits: $\beta 2(\text{*Y122} \rightarrow \text{W48} \rightarrow \text{Y356}) \rightarrow \alpha 2(\text{Y731} \rightarrow \text{Y730} \rightarrow \text{C439})$. The current model for RNR activity suggests that radical transport is strongly controlled by conformational gating. The C-terminal tail peptide (Y- β C19) of $\beta 2$ is the binding determinant of $\beta 2$ to $\alpha 2$ and contains the redox active Y356 residue. A photoRNR has been generated synthetically by appending a Re(bpy)(CO)₃CN ([Re]) photo-oxidant next to Y356 of the 20-mer peptide. Emission from the [Re] center dramatically increases upon peptide binding, serving as a probe for conformational dynamics and the protonation state of Y356. The diffusion coefficient of [Re]-Y- β C19 has been measured ($k_{\text{d1}} = 6.1 \times 10^{-7} \text{ cm}^{-1} \text{ s}^{-1}$), along with the dissociation rate constant for the [Re]-Y- β C19- $\alpha 2$ complex ($7000 \text{ s}^{-1} > k_{\text{off}} > 400 \text{ s}^{-1}$). Results from detailed time-resolved emission and absorption spectroscopy reveal biexponential kinetics, suggesting a large degree of conformational flexibility in the [Re]-Y- β C19- $\alpha 2$ complex that engenders partitioning of the N-terminus of the peptide into both bound and solvent-exposed fractions.

Amino acid radicals often serve as cofactors for substrate activation and vehicles for charge transport in enzymes (1). Free amino acid radicals in solution typically have micro- to millisecond lifetimes. Nature has evolved enzymes to manage both proton and electron equivalents so that the oxidative power of amino acid radical intermediates may be harnessed for chemical transformations over such disparate time scales (2). Oxidation of amino acids at physiological pH usually involves the loss of both a proton and an electron, implicating proton-coupled electron transfer (PCET)¹

as the redox mechanism (3–7). In a PCET event, proton tunneling is limited to short distances, usually within hydrogen bonds, whereas the electron, as the lighter particle, may tunnel over tens of ångströms (8–10). Enzymes have evolved to manage the different distance requirements of proton and electron tunneling to achieve efficient radical transport and catalysis (11).

Ribonucleotide reductase (RNR) serves as an exemplar for enzymes that derive their function from amino acid radicals (12). *E. coli* class I RNR contributes to DNA replication and repair by catalyzing the reduction of nucleoside diphosphates (NDPs) to deoxynucleoside diphosphates (dNDPs) (1, 13). The enzyme comprises two homodimeric subunits designated $\alpha 2$ and $\beta 2$, and a complex between the two is required for enzyme activity (14). $\alpha 2$ houses the NDP/ATP substrate/effector binding sites that control the specificity and rate of nucleotide reduction (15). $\beta 2$ harbors a diferric tyrosyl radical (*Y122) cofactor proposed to initiate nucleotide reduction by oxidizing a cysteine residue (C439) in the active site of $\alpha 2$ (16). Radical transport from *Y122 to C439 occurs over 35 Å (17) via a PCET amino acid radical transport pathway involving conserved amino acid residues $\beta 2(\text{*Y122} \rightarrow \text{W48} \rightarrow \text{Y356}) \rightarrow \alpha 2(\text{Y731} \rightarrow \text{Y730} \rightarrow \text{C439})$ (12, 18).

Photochemical RNRs (photoRNRs) have been designed to probe the intrinsic mechanistic steps attendant to radical transport between the tyrosines of the $\beta 2$ to $\alpha 2$ subunits (Y356 \rightarrow Y731) and along the $\alpha 2(\text{Y731} \rightarrow \text{Y730} \rightarrow \text{C439})$ pathway (19). In these constructs, $\alpha 2$ subunits are bound to the 20-mer, C-terminal peptide tail of $\beta 2$ (Y- β C19) containing a chemically appended

[†]These studies were supported by National Institutes of Health Grants GM29595 (J.S.) and GM47274 (D.G.N.). D.A.L. is a Jane Coffin Childs Memorial Fund for Medicinal Research Postdoctoral Fellow.

^{*}To whom correspondence should be addressed: Massachusetts Institute of Technology, 77 Massachusetts Ave., Cambridge, MA 02139-4307. Telephone: (617) 253-5537 (D.G.N.) or (617) 253-1814 (J.S.). Fax: (617) 253-7670 (D.G.N.) or (617) 258-7247 (J.S.). E-mail: nocera@mit.edu (D.G.N.) or stubbe@mit.edu (J.S.).

¹Abbreviations: $\alpha 2$, active site-containing subunit of RNR; Anq, anthraquinone; $\beta 2$, cofactor-containing subunit of RNR; β C19, 19-residue C-terminal peptide tail of $\beta 2$; BPA, 4-benzoylphenylalanine; CDP, cytidine 5'-diphosphate; dC, deoxycytidine; DOPA, 3,4-dihydroxyphenylalanine; ET, electron transfer; FPLC, fast protein liquid chromatography; MLCT, metal-to-ligand charge transfer; N₃NDP, 2'-azido-nucleotide 5'-diphosphate; PCET, proton-coupled electron transfer; PELDOR, pulsed electron–electron double resonance; photoRNR, photochemical ribonucleotide reductase; [Re], Re(bpy)(CO)₃CN; ³[Re]*, triplet MLCT excited state of [Re]; MP-FRAP, multiple-photon fluorescence recovery after photobleaching; RNR, ribonucleotide reductase; SA, specific activity; SF, stopped-flow; TA, transient absorption; TR, *E. coli* thioredoxin; TRR, *E. coli* thioredoxin reductase; Tris, tris(hydroxymethyl)aminomethane; Y*, tyrosyl radical; DLS, dynamic light scattering.

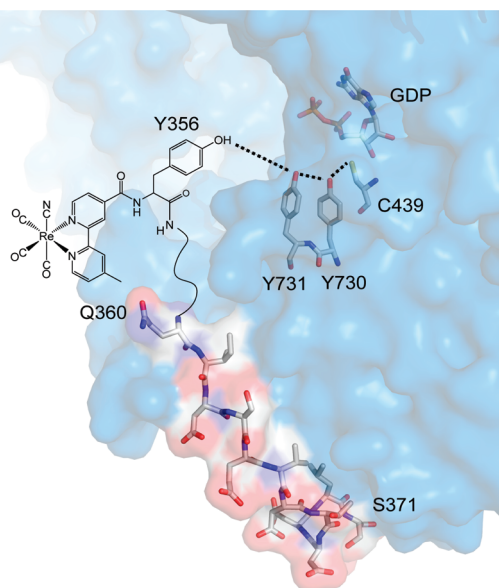


FIGURE 1: Molecular structure of [Re]-Y- β C19 bound to α 2. Peptide and protein coordinates are adapted from the X-ray structure of α 2 with the Y- β C19 peptide bound (18). The Y731–Y730 and Y730–C439 distances are 3.3 and 3.4 Å, respectively. Y- β C19 residues 356–359 are disordered in the structure; thus, the Y356–Y731 distance is unknown.

photo-oxidant (20–22). Y- β C19 is known to contain both the binding determinant of β 2 to α 2 (23, 24) and the redox active Y356 residue that facilitates radical transport between the two subunits (25–27). Figure 1 shows the X-ray crystal structure of α 2 highlighting the putative residues that comprise the radical transport pathway in this subunit, along with the bound Y- β C19 peptide (18). The N-terminal residues of Y- β C19, including the redox active “Y356” residue, are disordered in the structure. Excitation of the photo-oxidant appended proximal to Y356 on the peptide produces $^{\bullet}\text{Y356}$ (21, 22). When bound to the α 2 subunit in the presence of RNR substrate and effector, this phototriggered radical can be transported into the α 2 active site to initiate deoxynucleotide production. PhotoRNRs designed to date have been based on different photo-oxidants of tyrosine, including Trp (28), the benzophenone-containing unnatural amino acid (BPA) (21, 29), anthraquinone (Anq) (21), and the inorganic complex $\text{Re}^{\text{I}}(\text{bpy})(\text{CO})_2\text{CN}$ ([Re]) (30, 31). Of these various photoRNRs, the [Re]-based RNR affords the highest single-turnover yield (22). In model systems with tyrosine appended to the bpy ligand of [Re], the MLCT excited state of [Re] is a competent oxidant of the tyrosinate anion (Y^- , pH > 10) forming the $[\text{Re}^0]\text{-Y}^{\bullet}$ charge-separated state (30). Fluorotyrosine unnatural amino acids may be used to lower the pK_a of the phenolic proton (29) and thus enable photoactivity within the pH window for RNR activity ($6 < \text{pH} < 8.5$) (31). We have directly observed a $3,5\text{-F}_2\text{Y}^{\bullet}$ radical on a [Re]-3,5- $\text{F}_2\text{Y-}\beta$ C19 peptide and shown that the peptide bound to the Y731F- α 2 protein is competent for initiating RNR turnover at pH 7.5 and 8.2 (22).

With radical generation and competency established at the Y356 position, we have turned our attention toward a thorough characterization of Y356 on the peptide. We now report the utilization of the emission of the $[\text{Re}]^*$ excited state within the [Re]-Y- β C19- α 2 complex in probing the conformational dynamics of the N-terminus of the Y- β C19 peptide bound to α 2. We show that the $[\text{Re}]^*$ emission blue-shifts and increases

in intensity upon binding to α 2. Titration of the 3,5- F_2Y phenolic proton in the [Re]-3,5- $\text{F}_2\text{Y-}\beta$ C19- α 2 complex with base allows for modulation of the $[\text{Re}]^*$ emission intensity, as the deprotonated 3,5- F_2Y^- quenches the $[\text{Re}]^*$ excited state via electron transfer. Plots of the $[\text{Re}]^*$ emission intensity versus pH allow for determination of the pK_a of 3,5- F_2Y on the peptide bound to α 2. Stopped-flow and photobleaching experiments provide information about diffusion and binding rate constants between the peptide and the protein. Time-resolved emission spectroscopy reveals multiple solvation environments of the $[\text{Re}]^*$ excited state. These data, in combination with the X-ray data shown in Figure 1, support a model for a conformationally flexible N-terminus of the Y- β C19 peptide bound to α 2.

MATERIALS AND METHODS

Materials. The peptides [Re]-F- β C19, [Re]-3,5- $\text{F}_2\text{Y-}\beta$ C19, and [Re]-Y- β C19 were available from a previous study (22), and the synthesis of Ac-Y- β C19 has been described previously (20). The concentration of each [Re]-peptide stock solution was estimated by UV-vis absorption spectra using the known $\epsilon_{355} = 5300 \text{ M}^{-1} \text{ cm}^{-1}$ for the [Re]-3,5- $\text{F}_2\text{Y-OMe}$ dipeptide (31), and the concentration of Ac-Y- β C19 was estimated using $\epsilon_{280} = 1197 \text{ M}^{-1} \text{ cm}^{-1}$ for tyrosine (32). *Escherichia coli* thioredoxin (TR, SA of 40 units/mg), *E. coli* thioredoxin reductase (TRR, SA of 1800 units/mg), and *E. coli* β 2 (SA of 6800 nmol $\text{min}^{-1} \text{ mg}^{-1}$) were isolated as previously described (33). *E. coli* α 2 was isolated, purified, and prereduced according to an established procedure (21).

Steady State Emission Spectroscopy. Steady state emission spectra were recorded on an automated Photon Technology International (PTI) QM 4 fluorimeter equipped with a 150 W Xe arc lamp and a Hamamatsu R928 photomultiplier tube. Solutions (200 μL) containing [Re]-peptide and α 2 were placed in a 2 mm \times 10 mm quartz microcuvette and excited with 315 nm light focused along the 10 mm path length. Emission was collected at 90° to the excitation source and passed through a 450 nm long-pass filter prior to entering the detector housing. Emission spectra were recorded as a function of pH for solutions containing 20 μM α 2, 5.5 μM [Re]-3,5- $\text{F}_2\text{Y-}\beta$ C19, 50 mM buffer (either KPi or Tris), 15 mM Mg^{2+} , 3 mM ATP, and 1 mM CDP. Phosphate and Tris buffers were used in the pH ranges of 6.3–7.0 and 7.2–8.9, respectively.

Stopped-Flow Kinetics. Stopped-flow (SF) kinetic experiments were performed on an Applied Photophysics DX.17MV instrument equipped with the Pro-Data upgrade and an emission PMT. Samples were excited with $\lambda = 355 \text{ nm}$, and emission detection was limited to $\lambda > 455 \text{ nm}$ using a long-pass cutoff filter from Applied Photophysics Ltd. The temperature was maintained at 9°C with a Lauda RE106 circulating water bath. All experiments were performed in assay buffer [50 mM Tris, 15 mM MgSO_4 , 3 mM ATP, and 1 mM CDP (pH 7.6)]. Prior to each experiment, the instrument was flushed with copious amounts of water and then with assay buffer. [Re]-F- β C19 in one syringe was mixed with assay buffer in another syringe in equal volumes to yield a final concentration of 45 μM [Re]-F- β C19. This experiment provided the baseline [Re] emission of the [Re]-F- β C19 peptide. [Re]-F- β C19 and α 2 in one syringe were mixed with assay buffer in another syringe in equal volumes to yield final concentrations of 45 μM [Re]-F- β C19 and 1 μM α 2. The peptide emits more intensely when bound to the protein (vide infra); hence, these conditions provide the maximum emission expected from [Re] for this experiment. Finally, [Re]-F- β C19 and

$\alpha 2$ in one syringe were mixed with Ac-Y- β C19 in another syringe in equal volumes to yield final concentrations of 45 μ M [Re]-F- β C19, 1 μ M $\alpha 2$, and 450 μ M Ac-Y- β C19. Two thousand evenly spaced data points were collected over several time scales ranging from 50 ms to 20 s.

Analysis of [Re]-Y- β C19 Binding to $\alpha 2$. Binding of the [Re]-Y- β C19 peptide to $\alpha 2$ was monitored by steady state emission spectroscopy. Solutions of 5 μ M peptide were titrated with $\alpha 2$ from 0 to 65 μ M. Emission from [Re] did not significantly change at higher concentrations of $\alpha 2$; thus, at 65 μ M, we concluded that each molecule of $\alpha 2$ was bound to two [Re]-Y- β C19 peptide molecules. The fraction of bound peptide as a function of α concentration, $\chi_{\text{bound}}(\alpha)$, was then calculated from the equation

$$\chi_{\text{bound}}(\alpha) = \frac{I_{600}(\alpha) - I_{600}(0)}{I_{600}(130 \mu\text{M}) - I_{600}(0)} \quad (1)$$

where I_{600} is the emission intensity at 600 nm. Data were fit to the following simplified binding model:



where P is [Re]-Y- β C19. From this model, we can derive an expression for χ_{bound} (34):

$$\chi_{\text{bound}} = \frac{1}{1 + \frac{K_D}{\alpha}} \quad (3)$$

assuming that K_D is the same for binding of the first and second peptide to $\alpha 2$, as previously discussed (23). K_D is derived from a plot of χ_{bound} versus $[\alpha]$ and a fit of the data to eq 3.

Diffusion Coefficients. The diffusion coefficient of [Re]-Y- β C19 (at a concentration of 3.65 mM) was determined using Multi-Photon Fluorescence Recovery after Photobleaching (MP-FRAP) (35). The excitation source was a tunable mode-locked Ti:sapphire laser (Mai-Tai Broadband, Spectra-Physics, Mountain View, CA) at 800 nm. The beam was fed into a custom-built multiphoton microscope containing an Axioskop upright microscope (Carl Zeiss, Inc., Thornwood, NY) and Bio-Rad MRC-600 confocal laser scanner (Carl Zeiss, Inc.). For each measurement, the laser was focused with a 40 \times (0.75NA, Zeiss) water-immersion objective to a fixed spot (non-scanning) in the sample at low power (~ 5 – 10 mW at the sample) to monitor fluorescence in the absence of photobleaching. Photons were detected with a photomultiplier tube (H7421-40, Hamamatsu, Inc., Bridgewater, NJ) and binned using a multichannel scaler and averager (SR430, Stanford Research Systems, Sunnyvale, CA). An electro-optic modulator (KD*P Pockels cell, ConOptics, Danbury, CT) and digital delay generator (DG535, Stanford Research Systems) were used to rapidly modulate the laser power with custom-built hardware and a user interface developed in LabView (National Instruments, Austin, TX). In a single bleaching pulse, the laser power was increased briefly ($< 100 \mu$ s) to produce a more intense pulse of light (~ 40 – 60 mW at the sample), which caused irreversible photobleaching in the focal volume. The laser power was then returned to its low original value, and fluorescence recovery was monitored over several milliseconds. Because of the low concentration of fluorophores within the focal volume, the bleach and recovery process was repeated hundreds of times and fluorescence counts were summed into a single measurement to improve the signal-to-noise ratio. Diffusion coefficients were obtained by fitting a model one-component recovery curve to the

change in amplitude of fluorescence over time with nonlinear least-squares fitting incorporating a trust-region algorithm (35).

The diffusion coefficient of $\alpha 2$ (at a concentration of 8 μ M) was determined by dynamic light scattering (DLS) performed on a DynaPro dynamic light scatterer. The laser power and temperature were set to 37% and 25 $^{\circ}$ C, respectively. Each autocorrelation function (ACF) was acquired for 10 s and averaged over 10 measurements. The resulting ACF was fit using Dynamics V6 (version 6.7.7.9) from Wyatt Technology Corp. employing a non-negative least-squares fitting algorithm. Hydrodynamic radii were obtained from a mass-weighted size distribution analysis, and the reported value is the average of three measurements. The diffusion coefficient of $\alpha 2$, k_{d2} , was calculated with the Einstein–Stokes relationship

$$k_{d2} = \frac{k_B T}{6\pi\eta r} \quad (4)$$

where k_B is Boltzmann's constant, T is temperature (25 $^{\circ}$ C), η (~ 1 cP) is the viscosity of the solution, and r is the radius of $\alpha 2$. The radius obtained from DLS experiments was compared to the radius of a sphere with a volume equal to that of $\alpha 2$

$$r = \frac{\sqrt[3]{d_1 d_2 d_3}}{2} \quad (5)$$

where d_1 , d_2 , and d_3 are the diameters of $\alpha 2$ in the x , y , and z directions, respectively (36). Equation (5) is obtained from equating the volume of a sphere with the volume of an ellipsoid and solving for r .

Analysis of [Re]-Y- β C19 Binding to $\alpha 2$. The diffusion-limited rate constant, k_D , was determined from (37)

$$k_D = 4\pi(k_{d1} + k_{d2})R \quad (6)$$

where k_{d1} and k_{d2} are the diffusion coefficients of the [Re]-Y- β C19 peptide and $\alpha 2$, respectively, and R is the estimated radius of the binding site on $\alpha 2$. The binding site of the [Re]-Y- β C19- $\alpha 2$ complex was estimated from the crystal structure of $\alpha 2$ with Ac-Y-19mer (18). Only the 16 residues observed were used, and an effective radius (8.97 \AA) was calculated from the x , y , and z dimensions of the observed binding site (36.4, 15.4, and 10.3 \AA , respectively) using eq 5.

Time-Resolved Emission and Transient Absorption. Time-resolved emission measurements on the < 20 ns time scale were made with the frequency-doubled (400 nm) pump light provided by a Ti:sapphire laser system (100 fs pulse width) and collected on a Hamamatsu C4334 Streak Scope streak camera (38). Time-resolved emission measurements on the > 20 ns time scale were made with pump light provided by the third harmonic (355 nm) of an Infinity Nd:YAG laser (Coherent) running at 20 Hz (39). Nanosecond transient absorption (TA) measurements were taken with the same laser running at 10 Hz. The sample preparation and experimental setup were identical to those previously described (22).

To produce a transient absorption (TA) spectrum, a series of four spectra was taken: I_F (pump on/probe off), I (pump on/probe on), I_B (pump off/probe off), and I_0 (pump off/probe on). Transient spectra were corrected for fluorescence and background light using these spectra by the calculation $\Delta\text{OD} = \log[(I_0 - I_B)/(I - I_F)]$. For experiments involving $\alpha 2$, the spectra reported are an average of 125 of the four-spectrum sequences. Sample sizes were typically 200 μ L in a 2 mm \times 10 mm cuvette containing a Teflon-coated mini-stirbar. Both the white light and

pump beams were focused and overlapped to pass through the 2 mm wide window of the cuvette, providing a total path length of 1 cm. To provide optimal beam overlap, the pump beam was reflected off a small mirror in front of the collimating lens for the probe beam after the sample.

RESULTS

Photophysics and Photochemistry of [Re]-(F/Y/3,5-F₂Y)- β C19 Peptides. The quenching of the ³[Re]* excited state in the [Re]-3,5-F₂Y- β C19 peptide can be investigated with steady state emission spectroscopy. Figure 2 plots the emission spectra of the [Re] center as the pH of a solution of the [Re]-3,5-F₂Y- β C19 peptide is varied from 4.5 to 11.5. Between pH 4.5 and 5.0, the emission red-shifts and decreases in intensity. We ascribe these spectral changes to an alteration of the peptide conformation, as the carboxylic acid groups of Asp and Glu residues are typically deprotonated in this pH regime. Between pH 5 and 11.5, the emission energy and band shape do not change; however, the overall intensity of the band decreases. This emission quenching is consistent with deprotonation of the 3,5-F₂Y phenolic proton, which induces electron transfer from 3,5-F₂Y[−] to the proximate ³[Re]* excited state (31). By titrating the ³[Re]* emission intensity with pH, we obtain a pK_a value for 3,5-F₂Y when incorporated into the peptide of 7.3 ± 0.1, which is comparable to the pK_a of 7.2 for the Ac-3,5-F₂Y-NH₂ amino acid in solution (29).

The emission of the [Re] excited state on [Re]-(F/Y/3,5-F₂Y)- β C19 can be time-resolved to provide insight into the conformational homogeneity of the peptide. The emission decay of [Re]-3,5-F₂Y- β C19 at pH 10 fits to a biexponential decay function with $\tau_1 = 1.9$ ns (66%) and $\tau_2 = 10.7$ ns (34%) as does the emission decay of [Re]-Y- β C19 at pH 12 [$\tau_1 = 0.5$ ns (86%) and $\tau_2 = 3.0$ ns (14%)]. Both lifetime components for each peptide are faster compared to the emission lifetime of the [Re]-F- β C19 control peptide at all pH values or [Re]-Y- β C19 at pH < 10 ($\tau = 50 \pm 2$ or 62 ± 2 ns).

Binding of the [Re]-Y- β C19 Peptide to α 2. Peptide binding to α 2 may be probed by monitoring the emission energy of the ³[Re]* excited state. Figure 3 plots the emission spectra of a 5 μ M solution of the [Re]-Y- β C19 peptide as the α 2 concentration is increased from 0 to 65 μ M. When [Re]-Y- β C19 binds to α 2, the emission band blue-shifts and increases in intensity. This is consistent with partial desolvation of the [Re] chromophore upon binding to the protein (40, 41). Because there are two binding sites on each α 2 subunit (one on each α in the dimer) as shown in the crystal structure (18), the inset of Figure 3 plots the emission maxima as a function of α concentration. The fit of these data to the binding model described by eq 3 yields a dissociation constant, K_D , of 9 μ M. This value of K_D is comparable to the value obtained from competitive inhibition assay (23, 24) measurements of the binding of [Re]-Y- β C19 peptide to α 2 [$IC_{50} = 8 \mu$ M $\approx K_D$ (22)].

pK_a of 3,5-F₂Y356 Bound to α 2. The pK_a of 3,5-F₂Y on the peptide bound to α 2 may be ascertained by monitoring the emission intensity and lifetime of the ³[Re]* excited state. Figure 4 plots the emission intensity of a 5.5 μ M solution of [Re]-3,5-F₂Y- β C19 in the presence of 20 μ M α 2 as the pH is increased from 6.3 to 9.0. The dark gray spectra in the figure correspond to the emission of 5 μ M [Re]-3,5-F₂Y- β C19 in the absence of α 2 at pH 6.3 (top spectrum) and 9.0 (bottom spectrum) and re-emphasize the effect of peptide binding on the [Re] emission band at both pH 6.3 and 9.0. As the pH is titrated from 6.3 to 9.0 for the solution containing the bound peptide, the ³[Re]* emission intensity

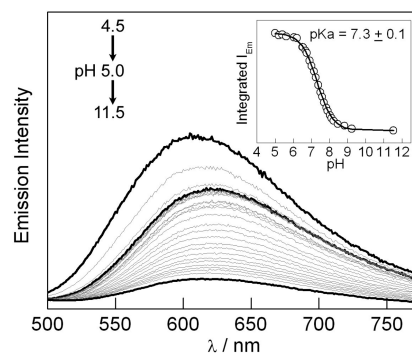


FIGURE 2: Emission spectra of [Re]-3,5-F₂Y- β C19 as a function of pH, which was titrated from 4.5 to 11.5. Black curves correspond to emission at pH 4.5, 5.0, and 11.5. The inset shows the pH titration curve of integrated emission intensity from pH 5.0 to 11.5.

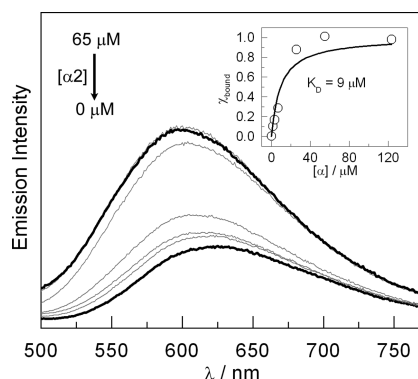


FIGURE 3: Emission spectra of [Re]-Y- β C19 (5 μ M) at pH 7.5 as the α 2 concentration is increased from 0 to 65 μ M. The inset shows the fraction of peptide bound as a function of α concentration (○) with a fit (—) to the binding model in eq 3.

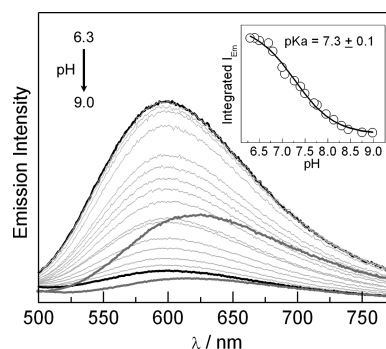


FIGURE 4: Emission spectra of [Re]-3,5-F₂Y- β C19 (5 μ M) and α 2 (20 μ M) as the pH is titrated from 6.3 to 9.0. The solid black curves correspond to the end points of the titration. The dark gray traces are spectra recorded at pH 6.3 (top spectrum) and pH 9.0 (bottom spectrum) in the absence of α 2. The inset shows the integrated emission intensity as a function of pH (○) with a fit (—) to the monoprotic titration curve.

decreases with an apparent pK_a of 7.3 ± 0.1. The same pK_a was obtained whether the integrated emission or emission maximum (at 600 or 650 nm) was plotted versus pH. As seen in Figure 2, deprotonation of the phenol of 3,5-F₂Y allows electron transfer to occur between 3,5-F₂Y[−] and ³[Re]*, resulting in a decrease in emission intensity. We thus attribute the emission quenching in Figure 4 to electron transfer between ³[Re]* and 3,5-F₂Y[−] on the peptide bound to α 2. Thus, the pK_a of the bound 3,5-F₂Y does not shift significantly from that of the unbound peptide in solution.

Kinetic Analysis of [Re]* Decay in [Re]-(F/Y)- β C19- α 2 Complexes. Time-resolved emission monitoring the decay

kinetics from the [Re] excited state ([Re]*) was used to further probe the homogeneity of the peptide- $\alpha 2$ binding interaction. For this experiment, 5 μM peptide and 20 μM $\alpha 2$ (with 3 mM ATP and at pH 7.5) were used to ensure that most of the peptide was bound. All experiments were performed in buffered solutions containing 20% glycerol, as this was previously shown to increase the yield of photochemical RNR turnover (22). Figure 5 plots the emission decay trace obtained at 600 nm for 5 μM [Re]-Y- βC19 and 20 μM $\alpha 2$. The same trace was obtained in the presence of 1 mM CDP substrate. Under all conditions investigated, the data were best fit with a biexponential decay function. One emission decay component was set equal to that of the free peptide while the other component was allowed to vary. We obtained decay components of 60 (63%) and 150 ns (37%), which were unaffected by the addition of 1 mM CDP substrate. These data reveal that the conformation of the peptide bound to $\alpha 2$ is heterogeneous, with multiple binding modes. For some binding modes, the [Re] unit may be solvated similar to that in free solution, while for others, the [Re] chromophore is partially desolvated, resulting in a blue-shifted emission energy with a longer emission lifetime.

TA spectroscopy was used to characterize the intermediate species produced upon laser excitation. The [Re]-F- βC19 - $\alpha 2$ system, with phenylalanine in place of tyrosine at position 356 of the peptide, was used as a control. Electron transfer photoproducts are not expected when tyrosine is replaced with phenylalanine because its oxidation by the [Re]* excited state is significantly endergonic (30). Figure 6 plots the TA spectra recorded for 100 μM solutions of [Re]-F- βC19 (top) and [Re]-Y- βC19 (bottom) in the presence of 135 μM $\alpha 2$, 1 mM CDP, and 3 mM ATP in 20% glycerol at pH 7.5. The spectra in both panels contain features at 380 and 480 nm and resemble that obtained for the peptides free in solution (Figure S1 of the Supporting Information). These spectra are assigned to the $^3[\text{Re}]^*$ excited state, as they are identical to that observed in [Re]-Y model compounds (30). For both peptides, the absorbance decay at 480 nm could be fit to a biexponential decay function with $\tau_1 = 62$ ns (55%) and $\tau_2 = 150$ ns (45%) for the [Re]-F- βC19 - $\alpha 2$ system and $\tau_1 = 62$ ns (62%) and $\tau_2 = 185$ ns (38%) for the [Re]-Y- βC19 - $\alpha 2$ system. These data are consistent with the time-resolved emission results discussed above that suggest the peptide binds to $\alpha 2$ in a heterogeneous fashion.

Dissociation Kinetics of the [Re]-(F/Y)- βC19 - $\alpha 2$ Complex. The goal of observing and measuring radical transfer processes from Y356 of modified peptides such as [Re]-Y- βC19 requires that the peptide remain bound to $\alpha 2$ for a sufficiently long time so that radical injection can occur. In other terms, the dissociation rate constant for the [Re]-Y- βC19 - $\alpha 2$ complex (k_{off}) must be slower than the PCET rate constant. To this end, we have undertaken experiments to measure the rates of association and dissociation of the peptide- $\alpha 2$ complex.

The data in Figure 3 shows that the emission of [Re]-Y- βC19 increases in the presence of $\alpha 2$, and thus, loss of emission intensity could provide a reasonable method for assessing the dissociation of the peptide from the [Re]-F- βC19 - $\alpha 2$ complex using stopped-flow spectroscopy. The baseline [Re] emission was determined by mixing Re-F- βC19 in one syringe with an equal volume of assay buffer in a second syringe to yield final concentrations of 45 μM . This baseline emission is shown by the black trace in Figure S2 of the Supporting Information. As a second control, $\alpha 2$ and Re-F- βC19 in one syringe were mixed with an equal volume of assay buffer from a second syringe to yield final

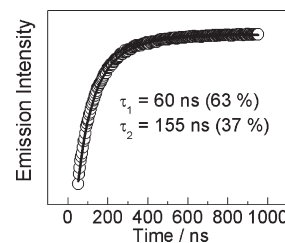


FIGURE 5: Time-resolved emission decay trace recorded at 600 nm for [Re]-Y- βC19 (5 μM) in the presence of $\alpha 2$ (20 μM) and ATP (3 mM).

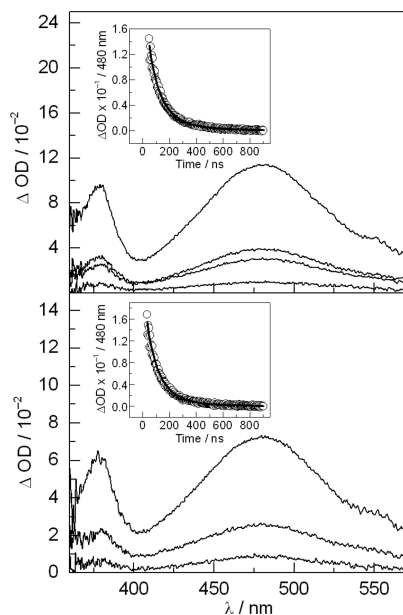


FIGURE 6: TA spectra recorded for 100 μM solutions of [Re]-F- βC19 (top) and [Re]-Y- βC19 (bottom) in the presence of 135 μM $\alpha 2$, 1 mM CDP, and 3 mM ATP in 20% glycerol at pH 7.5. Spectra were recorded at 65, 115, 215, and 415 ns (top) and at 115, 215, and 415 ns (bottom). Insets show single-wavelength absorbance kinetics data measured at 480 nm.

concentrations of 45 and 1 μM , respectively. As expected from Figure 3, the [Re] emission intensity (red trace in Figure S2) is enhanced relative to the baseline because of the binding of the peptide to $\alpha 2$. To monitor peptide dissociation, a competitive binding experiment was performed in which a Re-F- βC19 - $\alpha 2$ complex was mixed with a 10-fold excess of Ac-Y- βC19 . Subsequent to Re-F- βC19 dissociation, Ac-Y- βC19 outcompetes Re-F- βC19 for rebinding. Ac-Y- βC19 was chosen for this experiment since it is nonemissive and has a $K_d \approx 20$ μM (20). As shown by the green trace in Figure S2, the emission intensity of the [Re] peptide is rapidly decreased upon mixing. This observation is in accordance with the replacement of a Re-F- βC19 by Ac-Y- βC19 on $\alpha 2$. The rapid intensity loss suggests that the peptide dissociation occurs in the dead time of the instrument. This sets a lower limit for the off rate (k_{off}) at > 400 s^{-1} . Additionally, since $K_d = 9$ μM , a k_{on} of $> 4.4 \times 10^7$ $\text{M}^{-1} \text{s}^{-1}$ can be calculated.

Diffusion-Limited Rate Constants. The upper limit for k_{off} and k_{on} may be ascertained from the determination of the diffusion coefficient for Re-Y- βC19 and $\alpha 2$ and an estimate of the binding site between the two using eq 6. Multiple-photon fluorescence recovery after photobleaching (MP-FRAP) was used to determine the diffusion coefficient of Re-Y- βC19 (k_{d1}). Figure S3 of the Supporting Information shows the recovery

of the emission after an intense pulse of laser light was used to photobleach a defined area of the sample. The recovery is attributed to the diffusion of Re-Y- β C19 into the bleached area. A fit to the recovery curve yields a k_{d1} of $6.1 \times 10^{-7} \text{ cm}^2 \text{ s}^{-1}$ (35).

The diffusion coefficient of $\alpha 2$ (k_{d2}) was determined using the Einstein–Stokes relationship in eq 4 using the radius found by DLS and that estimated from the crystal structure of $\alpha 2$. The average hydrodynamic radius obtained from DLS from a mass-weighted size distribution analysis was 55.8 Å. The radius of $\alpha 2$ was also estimated to be 40.4 Å using eq 5 with d_1 , d_2 , and d_3 being equal to 100.7, 71.4, and 73.2 Å, respectively. These two radii yield k_{d2} values for $\alpha 2$ of 3.9×10^{-7} and $5.4 \times 10^{-7} \text{ cm}^2 \text{ s}^{-1}$, respectively.

The active site of the [Re]-(Y/F)- β C19- $\alpha 2$ complex was estimated from the crystal structure of Ac-Y- β C19 bound to $\alpha 2$ which has only 16 amino acid residues that are visible with X-ray crystallography (18). Using eq 5, the estimated radius of the active site was determined to be 8.97 Å. With eq 6, the diffusion-controlled rate constant for association of the [Re]-(Y/F)- β C19- $\alpha 2$ complex (k_{on}) was found to be $6.8\text{--}7.8 \times 10^8 \text{ M}^{-1} \text{ s}^{-1}$. Using a K_d of 9 μM , a limiting rate constant for dissociation (k_{off}) was computed to be between 6100 and 7000 s^{-1} . With these results and the SF kinetic data, the kinetics of association and dissociation for the [Re]-(Y/F)- β C19- $\alpha 2$ complex can be bracketed: $7.8 \times 10^8 \text{ M}^{-1} \text{ s}^{-1} > k_{on} > 4.4 \times 10^7 \text{ M}^{-1} \text{ s}^{-1}$, and $7000 \text{ s}^{-1} > k_{off} > 400 \text{ s}^{-1}$.

DISCUSSION

The [Re] complex within the [Re]-(F/Y/3,5-F₂Y)- β C19 peptide serves as a probe of both the peptide conformation and the pK_a of the adjacent Y residue. Excitation of [Re^I] produces a metal-to-ligand charge transfer (MLCT) excited state, in which a metal d-orbital electron is promoted to an orbital of π^* symmetry primarily localized on the bpy ligand, resulting in an effective Re^{II}(bpy^{•−}) electronic configuration. ³[Re^{II}(bpy^{•−})]* serves as a potent excited state oxidant ($E^\circ\{\text{[Re}^{\text{II}}(\text{bpy}^{\bullet-})]^*/[\text{Re}^{\text{I}}(\text{bpy}^{\bullet-})]\} = 1.59 \text{ V vs NHE (30)}$) that can oxidize deprotonated tyrosinate according to the mechanism



The emission of the photoexcited [Re] center is therefore quenched by the transfer of an electron from the adjacent tyrosine in [Re]-Y- β C19 upon deprotonation of the tyrosine phenol (22). Thus, monitoring of the emission band intensity as a function of pH probes the pK_a for the tyrosine phenol within the peptide and bound to $\alpha 2$. The solution pK_a value of tyrosine is maintained upon incorporation into the peptide and upon binding of the peptide to $\alpha 2$ [$pK_a(3,5\text{-F}_2\text{Y}) = 7.2$, $pK_a([\text{Re}]\text{-}3,5\text{-F}_2\text{Y-}\beta\text{C19}) = 7.3$, and $pK_a([\text{Re}]\text{-}3,5\text{-F}_2\text{Y-}\beta\text{C19-}\alpha 2) = 7.3$]. These results show that the photoRNR construct faithfully models RNR in that the pK_a of tyrosine at amino acid position 356 is unperturbed relative to the value in solution (42).

MLCT excitation of d^6 -polypyridyl complexes is associated with a marked increase in the molecular dipole because of the intramolecular charge separation. For this reason, the emission energy and intensity are strongly dependent upon the polarity of the surrounding environment (43). High-polarity solvents tend to lower the energy of the thermally equilibrated excited state, thus resulting in a red shift in the emission. Protic solvents, such as alcohols and water, also strongly quench the excited state lifetime through nonradiative decay mechanisms mediated by vibrational overlap of the excited state with the high-frequency

O–H stretch of the solvent (40). [Re] attached to the F_nY- β C19 peptide therefore serves as an effective probe of peptide conformation and binding to class I RNRs. Removal of water from the solvation sphere of [Re] upon peptide conformational changes or binding events serves to both blue-shift the energy of and increase the lifetime for the emission. The monotonic increase in the emission band to a higher energy with a concomitant increase in intensity (Figure 3) is consistent with the exclusion of water from the solvation sphere of the [Re] probe upon binding of the peptide to the protein. The shift in the emission profile with addition of the protein therefore provides a direct measure of peptide binding to $\alpha 2$. The similarity of the K_D of [Re]-Y- β C19 relative to that measured for Ac-Y- β C19 by competitive inhibition suggests that modification of the peptide with the [Re] moiety does not greatly perturb the interaction of the peptide with the protein. The multiple emission lifetimes observed for the [Re]-Y- β C19- $\alpha 2$ complex in the presence of RNR substrate and effector are consistent with multiple solvation environments of the [Re] chromophore, generally partitioning between protein-bound and solvent-exposed. Several other peptides containing photo-oxidants of different sizes and shapes have been generated, all of which bind to $\alpha 2$ with K_D values in the micromolar range (20, 21). In addition, the N-terminal peptide residues (356–360) are not located in the X-ray structure of the Ac-Y- β C19- $\alpha 2$ complex [Figure 1 (18, 44)]. Taken together, these results are consistent with a flexible peptide N-terminus when bound to $\alpha 2$.

The observation of conformational flexibility within the photoRNR provides a connection for conceptualizing the conformational gating of RNR activity at the molecular level. We have shown that the electron and proton are committed to a colinear pathway in $\alpha 2$ (21) for radical transport. The reaction rate for particle transfer is highly dependent on transfer distance because the electron and proton must tunnel. Whereas the electron can transfer over large distances, the proton cannot (9); hence, PCET may provide a basis for conformational gating in RNR. The binding of $\alpha 2$ to $\beta 2$ is known to trigger transport of a radical from [•]Y122 to Y356, but only in the presence of the RNR substrate and effector (26, 27). Conformational flexibility of the 356–360 region of $\beta 2$ within the $\alpha 2$ - $\beta 2$ complex would then allow the [•]Y356 radical to lock into the PCET pathway for radical transport across the subunit interface. Inasmuch as the [Re]-3,5-F₂Y- β C19- $\alpha 2$ complex has been shown to turn over upon irradiation (22), hole injection must be faster than the peptide off rate (k_{off}), which has now been determined to be in the range of 400–7000 s^{-1} . The conformational changes in the N-terminal peptide are likely to effect the efficient oxidation of Y731 in $\alpha 2$, making its detection challenging. Studies are now underway to examine how conformational changes in the N-terminal tail affect PCET in the photoRNR.

ACKNOWLEDGMENT

We thank Vikash P. Chauhan for his assistance with the MP-FRaP experiments.

SUPPORTING INFORMATION AVAILABLE

Transient absorption spectra of the [Re]-F- β C19 and [Re]-Y- β C19 peptides in aqueous solution, SF traces, and MP-FRaP trace. This material is available free of charge via the Internet at <http://pubs.acs.org>.

REFERENCES

- Stubbe, J., and van der Donk, W. A. (1998) Protein radicals in enzyme catalysis. *Chem. Rev.* 98, 705–762.
- Stubbe, J. (2003) Radicals with a controlled lifestyle. *Chem. Commun.*, 2511–2513.
- Cukier, R. I., and Nocera, D. G. (1998) Proton-coupled electron transfer. *Annu. Rev. Phys. Chem.* 49, 337–369.
- Mayer, J. M. (2004) Proton-coupled electron transfer: A reaction chemist's view. *Annu. Rev. Phys. Chem.* 55, 363–390.
- Hammes-Schiffer, S. (2001) Theoretical perspectives on proton-coupled electron transfer reactions. *Acc. Chem. Res.* 34, 273–281.
- Hodgkiss, J. M., Rosenthal, J., and Nocera, D. G. (2006) The relation between hydrogen atom transfer and proton-coupled electron transfer in model systems. In *Handbook of Hydrogen Transfer. Physical and Chemical Aspects of Hydrogen Transfer* (Hynes, J. T., Klinman, J. P., Limbach, H.-H., and Schowen, R. L., Eds.) pp 503–562, Wiley-VCH, Weinheim, Germany.
- Chang, C. J., Chang, M. C. Y., Damrauer, N. H., and Nocera, D. G. (2004) Proton-coupled electron transfer: A unifying mechanism for biological charge transport, amino acid radical initiation and propagation, and bond making/breaking reactions of water and oxygen. *Biochim. Biophys. Acta* 1655, 13–28.
- Moser, C. C., Keske, J. M., Warncke, K., Farid, R. S., and Dutton, P. L. (1992) Nature of biological electron transfer. *Nature* 355, 796–802.
- Reece, S. Y., and Nocera, D. G. (2009) Proton-coupled electron transfer: The engine that drives radical transport and catalysis in biology. In *Quantum Tunneling in Enzyme Catalyzed Reactions* (Scrutton, N. S., and Allemann, R., Eds.) Chapter 15, pp 351–383, Royal Society of Chemistry, London.
- Gray, H. B., and Winkler, J. R. (1996) Electron transfer in proteins. *Annu. Rev. Biochem.* 65, 537–561.
- Reece, S. Y., Hodgkiss, J. M., Stubbe, J., and Nocera, D. G. (2006) Proton-coupled electron transfer: The mechanistic underpinning for radical transport and catalysis in biology. *Philos. Trans. R. Soc. London, Ser. B* 361, 1351–1364.
- Stubbe, J., Nocera, D. G., Yee, C. S., and Chang, M. C. Y. (2003) Radical initiation in the class I ribonucleotide reductase: Long-range proton-coupled electron transfer? *Chem. Rev.* 103, 2167–2202.
- Jordan, A., and Reichard, P. (1998) Ribonucleotide reductases. *Annu. Rev. Biochem.* 67, 71–98.
- Thelander, L. (1973) Physicochemical characterization of ribonucleoside diphosphate reductase from *Escherichia coli*. *J. Biol. Chem.* 248, 4591–4601.
- Thelander, L., and Reichard, P. (1979) Reduction of ribonucleotides. *Annu. Rev. Biochem.* 48, 133–158.
- Stubbe, J., and Riggs-Gelasco, P. (1998) Harnessing free radicals: Formation and function of the tyrosyl radical in ribonucleotide reductase. *Trends Biochem. Sci.* 23, 438–443.
- Bennati, M., Robblee, J. H., Mugnaini, V., Stubbe, J., Freed, J. H., and Borbat, P. (2005) EPR distance measurements support a model for long-range radical initiation in *E. coli* ribonucleotide reductase. *J. Am. Chem. Soc.* 127, 15014–15015.
- Eriksson, M., Uhlin, U., Ramaswamy, S., Ekberg, M., Regnström, K., Sjöberg, B. M., and Eklund, H. (1997) Binding of allosteric effectors to ribonucleotide reductase protein R1: Reduction of active-site cysteines promotes substrate binding. *Structure* 5, 1077–1092.
- Reece, S. Y., and Nocera, D. G. (2009) Proton-coupled electron transfer in biology: Results from synergistic studies in model and natural systems. *Annu. Rev. Biochem.* 78, doi:10.1146/annurev.biochem.78.080207.092132.
- Chang, M. C. Y., Yee, C. S., Stubbe, J., and Nocera, D. G. (2004) Turning on ribonucleotide reductase by light-initiated amino acid radical generation. *Proc. Natl. Acad. Sci. U.S.A.* 101, 6882–6887.
- Reece, S. Y., Seyedsayamdost, M. R., Stubbe, J., and Nocera, D. G. (2007) Photoactive peptides for light-initiated tyrosyl radical generation and transport into ribonucleotide reductase. *J. Am. Chem. Soc.* 129, 8500–8509.
- Reece, S. Y., Seyedsayamdost, M. R., Stubbe, J., and Nocera, D. G. (2007) Direct observation of a transient tyrosine radical competent for initiating turnover in a photochemical ribonucleotide reductase. *J. Am. Chem. Soc.* 129, 13828–13830.
- Climent, I., Sjöberg, B. M., and Huang, C. Y. (1991) Carboxyl-terminal peptides as probes for *Escherichia coli* ribonucleotide reductase subunit interaction: Kinetic analysis of inhibition studies. *Biochemistry* 30, 5164–5171.
- Climent, I., Sjöberg, B. M., and Huang, C. Y. (1992) Site-directed mutagenesis and deletion of the carboxyl terminus of *Escherichia coli* ribonucleotide reductase protein R2. Effects on catalytic activity and subunit interaction. *Biochemistry* 31, 4801–4807.
- Seyedsayamdost, M. R., Yee, C. S., Reece, S. Y., Nocera, D. G., and Stubbe, J. (2006) pH rate profiles of F_NY356-R2s (*n* = 2, 3, 4) in *Escherichia coli* ribonucleotide reductase: Evidence that Y356 is a redox-active amino acid along the radical propagation pathway. *J. Am. Chem. Soc.* 128, 1562–1568.
- Seyedsayamdost, M. R., and Stubbe, J. (2006) Site-specific replacement of Y₃₅₆ with 3,4-dihydroxyphenylalanine in the β 2 subunit of *E. coli* ribonucleotide reductase. *J. Am. Chem. Soc.* 128, 2522–2523.
- Seyedsayamdost, M. R., and Stubbe, J. (2007) Forward and reverse electron transfer with the Y₃₅₆DOPA- β 2 heterodimer of *E. coli* ribonucleotide reductase. *J. Am. Chem. Soc.* 129, 2226–2227.
- Reece, S. Y., Stubbe, J., and Nocera, D. G. (2005) pH dependence of charge transfer between tryptophan and tyrosine in dipeptides. *Biochim. Biophys. Acta* 1706, 232–238.
- Seyedsayamdost, M. R., Reece, S. Y., Nocera, D. G., and Stubbe, J. (2006) Mono-, di-, tri-, and tetra-substituted fluorotyrosines: New probes for enzymes that use tyrosyl radicals in catalysis. *J. Am. Chem. Soc.* 128, 1569–1579.
- Reece, S. Y., and Nocera, D. G. (2005) Direct tyrosine oxidation using the MLCT excited states of rhenium polypyridyl complexes. *J. Am. Chem. Soc.* 127, 9448–9458.
- Reece, S. Y., Seyedsayamdost, M. R., Stubbe, J., and Nocera, D. G. (2006) Electron transfer reactions of fluorotyrosyl radicals. *J. Am. Chem. Soc.* 128, 13654–13655.
- Fasman, G. D. (1989) *Practical Handbook of Biochemistry and Molecular Biology*, CRC Press, Boca Raton, FL.
- Salowe, S., Bollinger, J. M. Jr., Ator, M., Stubbe, J., McCracken, J., Peisach, J., Samano, M. C., and Robins, M. J. (1993) Alternative model for mechanism-based inhibition of *Escherichia coli* ribonucleotide reductase by 2'-azido-2'-deoxyuridine 5'-diphosphate. *Biochemistry* 32, 12749–12760.
- Van Holde, K. E. (1985) *Physical Biochemistry*, 2nd ed., Prentice Hall, Englewood Cliffs, NJ.
- Brown, E. B., Wu, E. S., Zipfel, W., and Webb, W. W. (1999) Measurements of molecular diffusion in solution by multiphoton fluorescence photobleaching recovery. *Biophys. J.* 77, 2837–2849.
- Mussell, R. D., and Nocera, D. G. (1988) Effect of long-distance electron transfer on chemiluminescence efficiencies. *J. Am. Chem. Soc.* 110, 2764–2772.
- Steinfeld, J. I., Francisco, J. S., and Hase, W. L. (1999) Reactions in Solution. In *Chemical Kinetics and Dynamics*, 2nd ed., Chapter 4, pp 124–146, Prentice Hall, Upper Saddle River, NJ.
- Damrauer, N. H., Hodgkiss, J. M., Rosenthal, J., and Nocera, D. G. (2004) Observation of proton-coupled electron transfer by transient absorption spectroscopy in a hydrogen-bonded, porphyrin donor-acceptor assembly. *J. Phys. Chem. B* 108, 6315–6321.
- Loh, Z.-H., Miller, S. E., Chang, C. J., Carpenter, S. D., and Nocera, D. G. (2002) Excited-state dynamics of cofacial pacman porphyrins. *J. Phys. Chem. A* 106, 11700–11708.
- Chen, P., and Meyer, T. J. (1998) Medium effects on charge transfer in metal complexes. *Chem. Rev.* 98, 1439–1478.
- Blanco-Rodriguez, A. M., Busby, M., Gradiñaru, C., Crane, B. R., DiBilio, A. J., Matousek, P., Towrie, M., Leigh, B. S., Richards, J. H., Vlček, A., and Gray, H. B. (2006) Excited-state dynamics of structurally characterized [Re^I(CO)₃(phen)(HisX)]⁺ (X = 83, 109) *Pseudomonas aeruginosa* azurins in aqueous solution. *J. Am. Chem. Soc.* 128, 4365–4370.
- Yee, C. S., Seyedsayamdost, M. R., Chang, M. C. Y., Nocera, D. G., and Stubbe, J. (2003) Generation of the R2 subunit of ribonucleotide reductase by intein chemistry: Insertion of 3-nitrotyrosine at residue 356 as a probe of the radical initiation process. *Biochemistry* 42, 14541–14552.
- Caspar, J. V., and Meyer, T. J. (1983) Photochemistry of tris(2,2'-bipyridine)ruthenium²⁺ ion (Ru(bpy)₃²⁺). Solvent effects. *J. Am. Chem. Soc.* 105, 5583–5590.
- Uhlin, U., and Eklund, H. (1994) Structure of ribonucleotide reductase protein R1. *Nature* 370, 533–539.